KTH Engineering Sciences

Tunable Laser Diodes for Oxygen Sensing

Stefano Bertani

Master of Science Thesis
Laser Physics
Department of Applied Physics
KTH – Royal Institute of Technology
Stockholm, Sweden 2006

TRITA-FYS: 2006-21
ISSN: 0280-316X
ISRN: KTH/FYS/--06:21--SE

Abstract

The main objective of this work was to explore the potentials of diode lasers as sources of tunable light for spectroscopic applications. Two different external cavity configurations were developed, both working in the spectral region of the oxygen A-band, around 760nm.

The first one is based on the classical Littrow scheme used in transmission, where the frequency-selective element is a metal-coated (Ti-Au) silicone elastomer diffraction grating. This innovative component was conceived and realized specifically for the present work. The tuning of the system is achieved by simply stretching the grating. This is the very first time this technique is presented and the results obtained are encouraging.

The second configuration includes a fiber Bragg grating, which can be tuned either by temperature or mechanical strain. In the present work only the first alternative was demonstrated.

A measurement of atmospheric oxygen was also successfully performed.

Abstract

L'obiettivo principale del presente lavoro di tesi è stato quello di studiare le potenzialità dei diodi laser come sorgenti accordabili di luce per applicazioni spettroscopiche. Sono state realizzate due differenti configurazioni a cavità esterna, entrambe funzionanti nella regione spettrale della banda A dell'ossigeno, intorno a 760nm.

La prima configurazione è basata sul classico schema Littrow usato in trasmissione, dove l'elemento selezionatore di frequenza è un reticolo di diffrazione realizzato in silicone e rivestito di uno strato metallico (Ti-Au). Questo innovativo componente è stato concepito e realizzato specificamente per il presente lavoro. L'accordamento del sistema è ottenuto semplicemente allungando il reticolo. E' la prima volta che questa tecnica viene presentata ed i risultati ottenuti sono incoraggianti.

La seconda configurazione comprende un reticolo di Bragg in fibra, che può essere accordato sia per temperatura che per trazione meccanica. Nel presente lavoro solo la prima alternativa è stata dimostrata.

Inoltre una misurazione spettroscopica sull'ossigeno atmosferico è stata effettuata con successo.

Acknowledgements

First of all I would like to thank professor Fredrik Laurell, who gave me the opportunity to carry out such a nice research experience in his group. He is an inexhaustible fountain of ideas and he has been a great inspirer during my work.

I will never be able to thank enough Björn Jacobsson, for his continuous help and support. He assisted me all along the way, getting me out of troubles numberless times. Sharing the office with him has been really enjoyable too.

The help of Mårten Stjernström on the chemical aspects of my work has been extremely precious and deserves a big thanks.

Thanks to Valdas Pasiskevicius, who always had an illuminating answer to my questions.

Thanks to Jens Tellefsen, who always made me feel home and tried to stimulate my shy Swedish.

My gratitude goes also to all the other guys in the group: Carlota, Anna, Stefan H., Pär, Mikael, Junji, Stefan B., Jonas, Sandra. They all have been very nice and friendly to me during my stay, sharing their knowledge and giving me a hand whenever I needed it.

Thanks to my Italian supervisor, professor Stefano Taccheo, for his sensible advices and help.

Thanks to all my good friends, in Italy and in Sweden, for their support and encouragement especially in the difficult moments.

Finally, thanks to my family, for being always close to me with their love and support.

Contents

1 Introduction

Tunable lasers remained for years confined to the laboratories. Today, thanks especially to the development of the external cavity diode laser (ECDL), they have widespread applications in many fields. At present, ECDL systems are commercially available in different configurations, generally at relatively low cost and with high performance. Spectroscopic applications, such as environmental monitoring, represent a conspicuous part of the ECDL market and the interest in them is continuously increasing.

The present work explored the possibility to develop innovative ECDL configurations, focusing principally on their applications in laser absorption spectroscopy.

This report begins with a brief treatment of the principles of absorption spectroscopy, with a special eye on the oxygen case. The following two chapters give a theoretical description of diffraction gratings and fiber Bragg gratings, focusing on the aspects that are more relevant for the involved applications. Chapter 5 deals with diode lasers, giving first a general overview and then describing more in depth the behavior of external cavity diode lasers (ECDLs). Finally, the description and characterization of each experimental setup is presented, together with the achieved results.

2 Laser Absorption spectroscopy

Trace gas detection is an important aspect of present-day environmental technological research. Laser absorption spectroscopy allows to determine quantitatively the concentration, temperature and pressure of a gas, from a measured absorption spectrum[1]. In this Chapter a brief review of the fundamental theoretical background is presented.

2.1 Molecular spectra

Every molecule has its own characteristic spectrum, i.e. it has specific wavelengths at which it can either absorb or emit light. As in the case of single atoms, when a molecule goes from a certain energy level to a lower one, the energy difference will appear as a photon with frequency $\nu = (E'' - E')/\hbar$. In case of absorption, this process is obviously inverted.

The energy levels of a molecule come not only from its electronic configuration, but also from its rotation and from the vibrations of its atoms around their equilibrium position. To each electronic level corresponds thus a multitude of vibrational levels, and for each of them we have a set of rotational levels. The spectrum associated with a specific electronic transition will be a collection of lines resulting from the transitions between the two sets of vibro-rotational levels associated with each electronic level, according to the selection rules for the different kinds of transitions. There can though exist transitions that do not involve a change in the electronic state, being simply vibro-rotational or pure rotational.

In the following paragraph a brief analysis of the different kinds of transitions is presented.

2.1.1 Electronic and vibro-rotational transitions

Because of the high complexity of the interactions involved, the structures of the electronic energy levels of a molecule are extremely complicated. As a matter of fact, one has to take into account not only the mutual interactions between the electrons of each atom, but also the interactions with the electrons and nuclei of the other atoms of the molecule. In general, the quantum mechanical treatment follows quite closely the one for a single atom[2]. The orbital angular momentum quantum number is indicated with the symbol Λ, while the electronic states are identified by Greek letters, as it is shown here below.

$$\begin{array}{rcccc} \Lambda: & 0 & 1 & 2 & 3 \\ \textit{electronic state}: & \Sigma & \Pi & \Delta & \Phi \end{array}$$

The spin quantum number is instead indicated with S and, as in the case of atoms, it determines the multiplicity (2S+1) of the electronic state. The

selection rules for electronic transitions are:

$$\Delta\Lambda = 0, \pm 1 \tag{2.1}$$

$$\Delta S = 0 \tag{2.2}$$

For a simple treatment of the vibrational levels, it is worth to consider a biatomic molecule and write its potential energy using the parabolic approximation:

$$V(x) = \frac{1}{2}kx^2$$

where $x = r - r_{eq}$.The allowed energy levels are then simply:

$$E_v = (v + \frac{1}{2})\hbar\omega$$

with $v = 0, 1, 2, 3...$
$\mu = \frac{m_1+m_2}{m_1 m_2}$ is the reduced mass of the molecule and $\omega = \sqrt{(\frac{k}{\mu})}$. According to this simple model the vibrational levels are thus equally spaced. This is just a simple approximation, which loses accuracy as the vibrational energy increases and the atoms are subject to considerable displacement with respect to their equilibrium positions. P. M. Morse derived an expression for the energy that describes quite accurately the real behavior:

$$V(x) = D_{eq}[1 - e^{-a(r-r_{eq})}]^2$$

where $a = \sqrt{\frac{k}{2D_{eq}}}$ and $D_{eq}$is the depth of the potential minimum. Solving the Schrödinger equation using this expression for the potential, one gets the following energy levels:

$$E_v = (v + \frac{1}{2})\hbar\omega + (v + \frac{1}{2})^2 x_e \hbar\omega \tag{2.3}$$

where ω is the vibrations frequency in the harmonic potential, and $x_e = \frac{a^2\hbar}{2\mu\omega}$ is the first anharmonicity constant. For the simple harmonic oscillator the selection rule is:

$$\Delta v = \pm 1 \tag{2.4}$$

that taking into consideration anharmonicity becomes:

$$\Delta v = \pm 1, \pm 2, \pm 3... \tag{2.5}$$

The transitions with $\Delta v = \pm 2, \pm 3...$ are called overtones and are generally much weaker than the fundamental ones.

As already pointed out, to each vibrational level corresponds a set of rotational sublevels. Being

$$E_{rot} = J(J+1)\hbar c + K^2(C - B)\hbar c \tag{2.6}$$

the values of the rotational energy levels, the selection rule for the rotational transition associated to the vibrational one is:

$$\Delta J = \pm 1 \tag{2.7}$$

However, under some particular circumstances, we can also have $\Delta J = 0$. According to the variation of the angular momentum quantum number J, it is common to divide the vibro-rotational spectrum into three branches: the P branch ($\Delta J = -1$), the Q branch ($\Delta J = 0$) and the R branch ($\Delta J = 1$).

2.1.2 Electric-dipole vs. magnetic-dipole transitions

In order to interact with electromagnetic radiation, the electric-dipole moment of a molecule has to change when the mean distance between its atoms varies. However, in the case of homonuclear biatomic molecules, a change in vibrational level does not affect the value of the electric-dipole moment, which remains equal to zero. Such molecules usually do not have a vibrational spectrum and are said to be infrared inactive. To explain the existence of the vibrational transitions of oxygen we then need to take into consideration the magnetic dipole[3]. An atom or a molecule may in fact have both an electric and a magnetic-dipole moment, which in turn may have static and oscillatory components. The components of the magnetic-dipole moments are mainly a result of the quantum current distributions of the atomic or molecular system, with some minor contributions due to the spin of the orbiting electrons and of the nucleus. The static components are due to single eigenstates, while the oscillating ones are brought by pairs of eigenstates. We can thus observe transitions between the sublevels of two different vibrational levels, such that their electric-dipole moment is zero while the magnetic one is not. As a matter of fact, there is a significant number of visible and infrared transitions that are of magnetic-dipole character.

2.1.3 The oxygen A-band

The A-band of molecular oxygen(O_2), which lies around 760nm, is often chosen for spectroscopic measurements as there are not other species that absorb significantly in that region of the atmospheric spectrum. This was also the choice made in the present work.
The electronic transition involved is:

$$b^1\Sigma_g^+ \leftarrow X^3\Sigma_g^- \tag{2.8}$$

In particular, the A-band (Figure 2.1) results from the branch:

$$b^1\Sigma_g^+(v=0) \leftarrow X^3\Sigma_g^-(v=0) \tag{2.9}$$

One can notice that this transition does not respect the selection rule (2.2), occurring between a triplet(S=1) and a singlet(S=0) state. When such spin

forbidden transitions take place, they are sometimes referred to as intersystem crossings. This transition is said to be "weakly magnetic dipole allowed", thanks to a quite strong spin-orbit coupling between the $b^1\Sigma_g^+$ state and the lowest spin component of the $X^3\Sigma_g^-$ state[4][5][6].

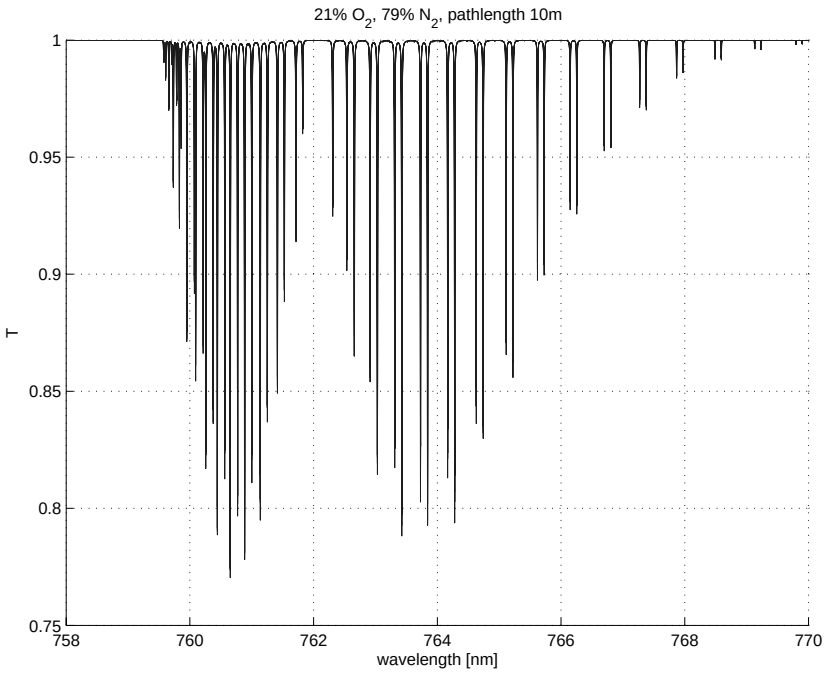

Figure 2.1. *The oxygen absorption A-band[7].*

2.2 The Beer-Lambert law

Laser absorption spectroscopy consists in observing the light after it has passed trough a medium, in our case a gas or a mixture of gases. Its intensity $I(\nu)$ at frequency ν will be attenuated exponentially, according to the Beer-Lambert law:

$$I(\nu) = I_0(\nu)\exp[-\sigma(\nu)NL] \tag{2.10}$$

where $I_0(\nu)$ is the original intensity, $\sigma(\nu)$ is the absorption cross-section, N the concentration of the absorbing species and L the length of the path through the medium. The absorption cross-section can in turn be expressed as a function of a line-strength S and a line-shape function $\Phi(\nu - \nu_0)$ according to:

$$\sigma(\nu) = S\Phi(\nu - \nu_0) \tag{2.11}$$

where ν_0 is the frequency at the line center and $\Phi(\nu - \nu_0)$ is normalized so that

$$\int_{\nu} \Phi(\nu - \nu_0) d\nu \equiv 1 \tag{2.12}$$

It is common to introduce the absorption coefficient as $\alpha(\nu) = \sigma(\nu)N$. If there are many species absorbing in the same region the absorption coefficient assumes a more complex form:

$$\alpha(\nu) = P \sum_{j=1}^{K} X_j \Phi_{i,j}(\nu) \sum_{i=1}^{M_j} S_{i,j}(T) \tag{2.13}$$

where P is the total pressure, X_j the mole fraction of the species j, K the total number of species, $S_{i,j}$ and $\Phi_{i,j}$ the line-strength and line-shape of a particular transition i of the species j, respectively. However, as in atmospheric air there is no significant absorption around 760 nm from any species but oxygen, we can keep the model simple.

2.3 Linewidth broadening

There exist different mechanisms that contribute to broaden the linewidth of every absorption line, which can be classified either in homogeneous or inhomogeneous ones. The former ones affect all the molecules in the same way, while the latter ones act in different ways for different subgroups of molecules. The basic broadening mechanism is always present and is a direct result of the Heisenberg uncertainty relation. The lifetime in every level is finite and this implies to have energy levels with a finite width, according to $\Delta t \cdot \Delta E \geq \frac{\hbar}{2}$, which in turn results into a broadened absorption line. This broadening, which is obviously homogeneous, has a Lorentzian line shape but it is always very weak (0.1-100Mhz) compared to the other mechanisms. The two significant mechanisms that we have to take into consideration are Doppler and collisional broadening.

The first one is due to the thermal motion of the absorbing molecules and produces a lineshape that is described by a Gaussian function:

$$\Phi_D(\nu - \nu_0) = \frac{1}{\Delta\nu_D} \sqrt{\frac{\ln 2}{\pi}} \exp[-\frac{\ln 2(\nu - \nu_0)^2}{\Delta\nu_D^2}] \tag{2.14}$$

It is the dominating mechanism at low pressure (<10 Torr) and has a halfwidth $\Delta\nu$ that increases with temperature according to:

$$\Delta\nu_D = \nu_0 \sqrt{\frac{2kT}{Mc^2} \ln 2} \tag{2.15}$$

where k is the Boltzmann constant, T the absolute temperature, M the molecular mass and c the speed of light. It is obviously an inhomogeneous mechanism.

Collisional (or pressure) broadening is the consequence of the shortening of the upper-level lifetime due to impacts between the molecules. It is the mechanism that dominates at high pressures (>100 Torr) and, being homogeneous, leads to a Lorentzian line shape:

$$\Phi_L(\nu - \nu_0) = \frac{\Delta\nu_L}{\pi} \frac{1}{(\nu - \nu_0)^2 + \Delta\nu_L^2} \tag{2.16}$$

with a pressure-dependent halfwidth given by

$$\Delta\nu_L = \sum_i \gamma_i p_i \tag{2.17}$$

where γ_i are the pressure broadening coefficients and p_i the partial pressures of the species present in the absorbing volume.

In an intermediate regime (10-100 Torr), known as Voigt regime, the effects of Doppler and collisional broadening are comparable and the resulting line shape comes from a convolution of the two. There is not an exact formula for the Voigt halfwidth. However, it is often sufficient to estimate it as:

$$\Delta\nu_V = \sqrt{(\Delta\nu_D^2 + \Delta\nu_L^2)} \tag{2.18}$$

3 Diffraction gratings

A diffraction grating is a collection of fine and parallel grooves, equally spaced on a reflective or transparent substrate. Its fundamental value lies in its ability to separate a polychromatic incident light beam into its monochromatic components. The first practical diffraction gratings were made in 1821 by Joseph von Fraunhofer that also derived the equations governing their behavior. His devices were good enough to resolve the sodium D lines. The quality of diffraction gratings was continuously improved in the following decades, thanks especially to the work of Nobert, Rutherfurd and Rowland. In the first half of the past century diffraction grating were already regarded as elements of primary importance for spectroscopic work. Nowadays a huge variety of diffraction gratings are commercially available, with up to 12000 lines/mm. In the present work, the manufacturing and characterization of experimental silicone gratings is presented.

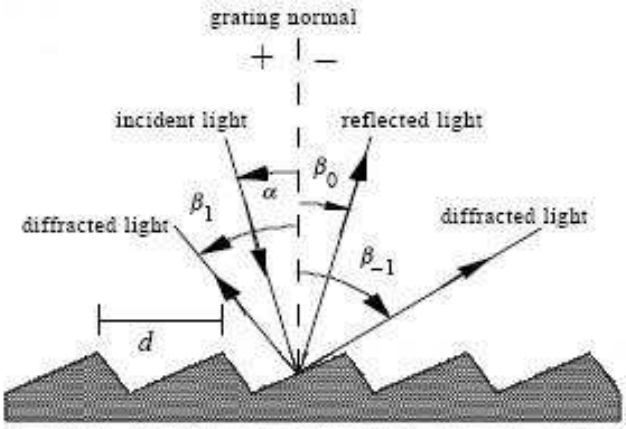

Figure 3.1. *Diffraction by a reflection grating.*

3.1 The grating equation

A beam of monochromatic light incident on a grating will be diffracted into one or several discrete directions. Such directions depend on the groove frequency of the grating and on the wavelength and incidence angle of the beam, according to:

$$m\lambda = d(\sin\alpha + \sin\beta_m) \tag{3.1}$$

which is known as the grating equation. The integer m is the diffraction order and d is the grooves spacing. For a reflection grating, the incidence angle α and the angle β_m of the m-th order diffracted beam are assumed

positive if measured counter-clockwise from the grating normal. In case of a transmission grating this convention is reversed, i.e. the angles of the transmitted beams are assumed positive if measured clockwise from the grating normal. In Figure 3.1 it is shown a graphical representation of diffraction by a reflection grating.
It is obviously possible to produce diffraction gratings that diffract light partly in reflection and partly in transmission, as it has been done in this work.

The grating equation (3.1) is valid in the ordinary case, when all the rays lie in one plane perpendicular to the grooves. However, if the incident beam doesn't satisfy this condition, equation (3.1) assumes the more general form:

$$m\lambda = d\cos\psi(\sin\alpha + \sin\beta_m) \tag{3.2}$$

where ψ is the angle between the incident beam and the plane perpendicular to the grooves. When $\psi \neq 0$, the diffracted beams lie on a cone rather than in a plane.
From the grating equation, we easily deduce that the only possible diffracted orders are those for which $|m\lambda/d| < 2$. The zero order will thus always exist, representing for many applications an useless waste of light. The other orders can be either positive($\beta > -\alpha$, taking $\alpha > 0$) or negative($\beta < -\alpha$, taking $\alpha > 0$).
Often a diffraction grating is used in the so-called Littrow configuration, where one diffraction order (usually the first one) is sent back in the direction of the incoming beam. In this case equation (3.1) becomes simply:

$$m\lambda = 2d\sin\alpha \tag{3.3}$$

3.2 Dispersion and resolving power

The ability of a grating to separate light of different wavelength can be evaluated through its angular dispersion. It is simply obtained differentiating the grating equation, keeping the incident angle α constant:

$$D = \frac{\mathrm{d}\beta}{\mathrm{d}\lambda} = \frac{m}{d\cos\beta} \tag{3.4}$$

To achieve high angular dispersion it is thus possible to use either a grating with high groove frequency, or a coarse-pitch grating in high diffraction order. The first choice is usually preferred, as it assures a larger free spectral range, which is the largest wavelength interval in a given order for which there is no superposition with light from adjacent orders.
A measure of the dispersion ability of a grating is the resolving power, defined as:

$$R = \frac{\lambda}{\Delta\lambda} \tag{3.5}$$

where $\Delta\lambda$ is the limit of resolution, i.e. the minimum difference in wavelength between two spectral lines of equal intensity that can be detected as separate. According to the Rayleigh criterion, two spectral peaks are considered resolved if the distance between them is such that the maximum of the first one falls on the first minimum of the second one. The resolving power can thus be rewritten as:

$$R = mN \tag{3.6}$$

where m is the diffraction order and N is the number of grooves that are illuminated. The use of a fine-pitch grating appears again highly convenient, especially for laser applications, where one usually wants to work with small beams that illuminate just a small region of the grating.

3.3 Efficiency of diffraction gratings

Efficiency is a fundamental characteristic of a diffraction grating. It is usually calculated as the ratio between the intensity diffracted to the considered order and the total intensity of the incident monochromatic light(absolute efficiency). Unfortunately, efficiency is also a very difficult characteristic to control, being generally a rather complex function of wavelength and polarization of the incident light, which depends on the material, the groove frequency and the shape of the grooves.

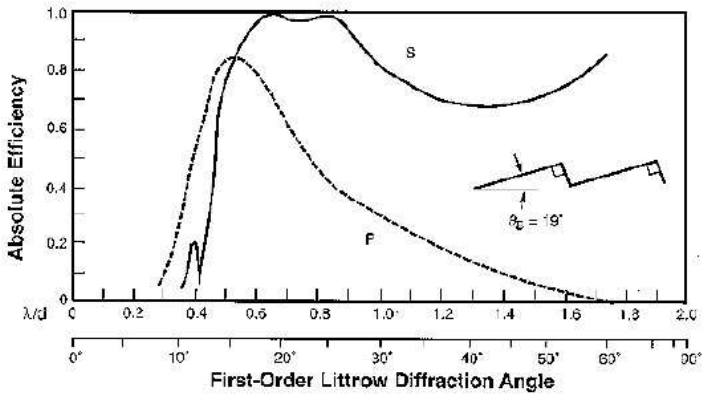

Figure 3.2. *First-order theoretical efficiency curve for a triangular-groove grating with 19° blaze angle in Littrow mounting[8].*

The choice of a triangular groove profile allows to maximize the efficiency of a single diffraction order for a specific wavelength. Such gratings are said to be blazed. Their groove profile is usually calculated for the Littrow condition, so that the groove angle gives a specular reflection in the same direction of the first diffracted order. The shape of the efficiency curves changes significantly with the blaze angle in a complex fashion. Theoretically, it is

possible to reach an efficiency as high as 100% for a specific wavelength and polarization.

Gratings with a sinusoidal groove profile show generally flatter efficiency curves, which depend strongly by the groove modulation μ, defined as:

$$\mu = h/d$$

where h is the groove height and d the groove spacing.

As one can notice in Figure 3.3, the efficiency curve of a metal-coated grating can present abrupt changes in some wavelength intervals. In the classical mount ($\psi = 0$), these anomalies appear only for TM polarization, i.e. when the electric vector is perpendicular to the grating grooves. They are named after R.W.Wood, who first observed them in 1902. However, their explanation came only many decades later and it involves a physical process known as surface plasmon resonance. Surface plasmons are a fundamental excitation of a metal-dielectric interface, characterized by an oscillation of charge density in the metal. Under some circumstances, surface plasmons can couple with electromagnetic waves, resulting in the so-called surface plasmon-polaritons and thus giving rise to the anomalies in the gratings efficiency curve.

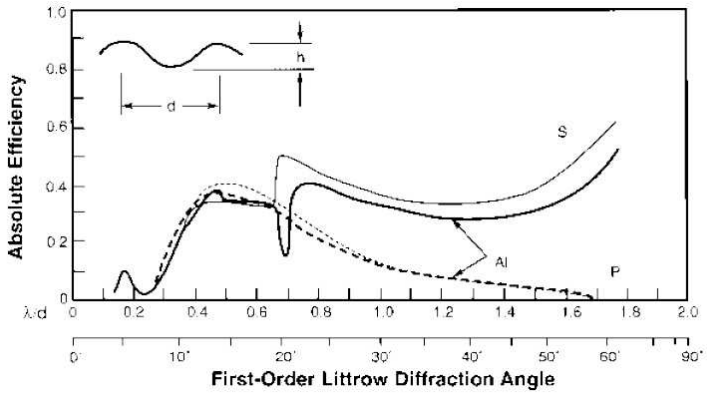

Figure 3.3. *First-order theoretical efficiency curve for a sinusoidal-groove grating with $\mu = 0.14$ in Littrow mounting.The light curves are for an ideal perfectly conducting surface[8].*

Moreover, metal-coated gratings suffers the consequences of the finite conductivity of the metal. The effects appear only for wavelengths below 1 μm and, for TE polarization, consist just in a reduction of efficiency , while for TM polarization a more complex behavior can arise.

For a complete treatment of diffraction gratings the reader is suggested to see [8].

A long time and many attempts have been dedicated to optimize the efficiency of the silicone gratings manufactured for the purposes of the present

work. Being simply molded replicas, the only parameters that could be changed to optimize their efficiency were the material and the thickness of the coating layer. Since these gratings have to work in Littrow configuration, the goal was to maximize the efficiency in the first reflected diffraction order, keeping enough power in the zero transmitted order, which has to be the detectable output of the system described in Chapter 6. The zero reflected order and the first transmitted one are, in this system, simply a waste of light.

3.4 Silicone gratings

The need for a partially transmitting diffraction grating with the desired efficiency distribution led to the development of molded silicone gratings. Such gratings turned out to be very cheap and of high quality. Moreover, they exhibit interesting elastic properties that were exploited in the Littrow-like setup described in Chapter 6.

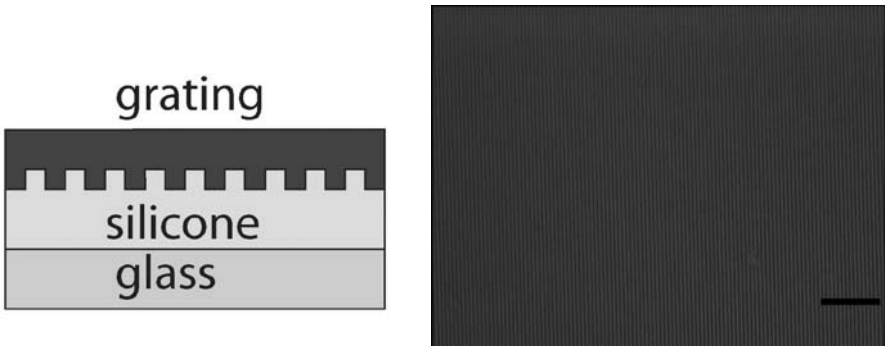

(a) Schematic drawing of the silicone gratings manufacturing principle. *(b) Picture of a metal coated silicone grating, obtained with a microscope at 100X.*

Figure 3.4

3.4.1 Manufacturing

The first step is to treat the glass substrate with Sigmacoat, to make easier the later removal of the grating from it. The material used to mould the grating is a silicone elastomer (Sylgard 184), which has to be mixed with 10% of curing agent. Before use, the air bubbles have to be completely removed. The mixture is thus put into lower pressure, with the help of a small hose connected to a simple hydraulic system, and dipped in an ultrasound degassing bath for about 10 minutes. The mixture is then poured on to the glass substrate and the master mould, which is a standard reflection grating, is laid face down on the top. To control the thickness of the silicone, the edges of the master mould lie on two microscope slides. This assembly is

then put in a oven at 85°C for 100 minutes. After it has cooled down, the molded grating can be removed, with the help of a scalpel.

3.4.2 Metal coating and efficiency

As it is shown in Figure 3.5, most of the light incident on a bare silicone grating goes into the zero transmitted order. To improve the reflectivity, the grating was thus metal coated. Many experiments have been made, using different metals and thicknesses. The best results were obtained using an electron beam evaporation system, depositing first a thin Ti layer(2nm), which improves the adhesion of the subsequent layer of Au(30nm). The efficiency of these gratings at 760nm is shown in Figure 3.6 (sample 4 and 5).

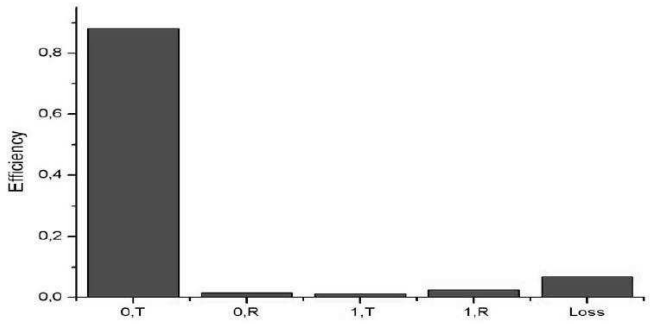

Figure 3.5. *Efficiency in the different orders of an uncoated silicone grating at 760nm in Littrow configuration for TM polarization.*

The efficiency of the best grating realized (sample 5) was measured also with a diode at 970nm. At this wavelength, the efficiency for the first reflected order is 70% for TM polarization and 6% for TE polarization.

Measurements of the grating profile has been carried out with an atomic force microscope(AFM) in contact mode, whose conical tip has a full angle of 30 degrees and a length of 20 microns. The results for both a bare silicone grating and a Ti-Au coated silicone grating are reported in Figure 3.7. The profiles appears clearly sinusoidal with a groove modulation $\mu \simeq 0.25$. The spatial period was measured to be about 0.55μm, which corresponds to a groove frequency of about 1800 lines/mm.

It is interesting to notice how the measured values of the efficiency at 760nm and 970nm for the coated gratings fit qualitatively the theoretical curve in Figure 3.3 for a sinusoidal-groove grating.

It has to be reported that in the same period of time in which the work presented here was going on, a paper was published describing the use of a

similar silicone grating (but produced with a different technique) as a light scanner in transmission[9].

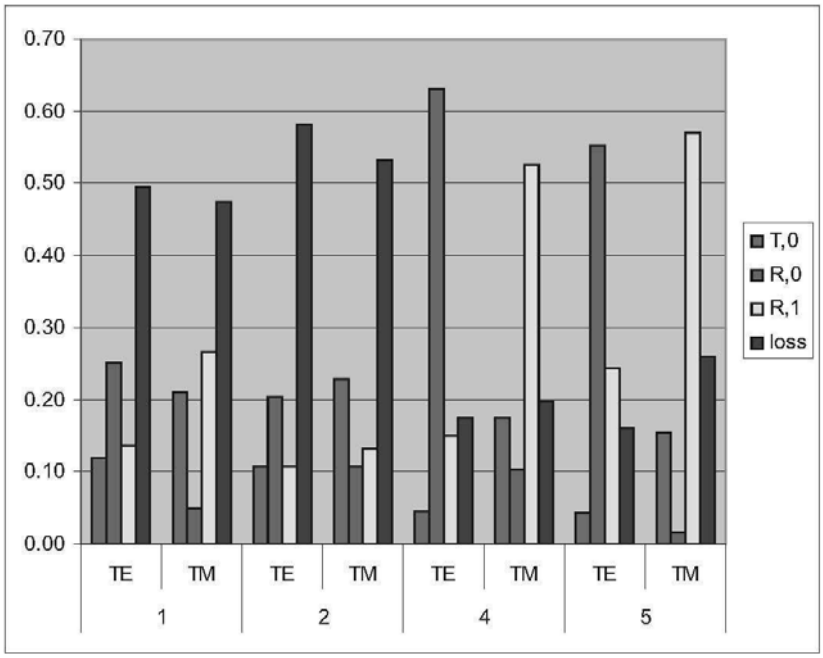

Figure 3.6. *Efficiency in the different orders of the metal-coated silicone gratings at 760nm. Samples number 1 and 2 are coated with a 2nm titanium layer and a 15nm gold layer, while number 4 and 5 with 2nm titanium and 30nm gold.*

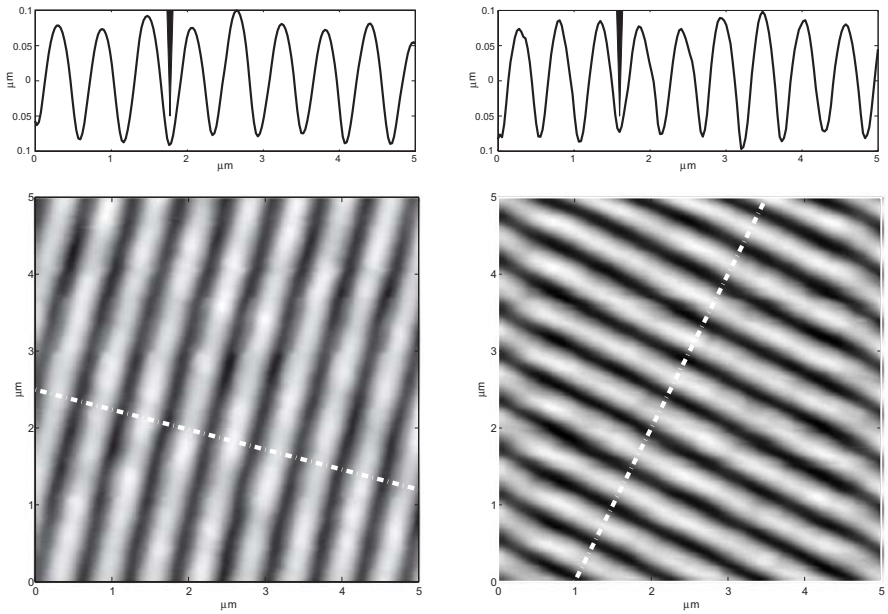

(a) *Bare silicone grating.* **(b)** *Ti-Au coated silicone grating.*

Figure 3.7. *Profile measurements carried out with an atomic force microscope (AFM) in contact mode. The dash-dotted line in the lower part of each figure indicates where the vertical section in the upper part is taken. In the upper part the filled black triangle shows the size of the scanning tip to scale.*

4 Fiber Bragg Gratings

A fiber Bragg grating consists of a periodic modulation of the effective refractive index in the core of an optical fiber. Its development was made possible by the discovery in 1978 of the photosensitivity of optical fibers, which, as many other important discoveries in history, occurred by accident.

4.1 Manufacturing of FBGs

The manufacturing of fiber Bragg gratings typically involves the illumination of the core material with ultraviolet laser light (e.g. from a KrF(248 nm) or ArF(193 nm) excimer laser), which induces some structural changes, giving rise to a permanent modification of the refractive index. The photosensitivity of the core glass is strongly dependent on the chemical composition and the UV wavelength: for silica glass it is very weak, while germanosilicate glass exhibits a much higher effect, allowing to achieve a refractive index difference up to about 10^{-3}. Loading the fiber with hydrogen it is possible to obtain a further increase of photosensitivity.

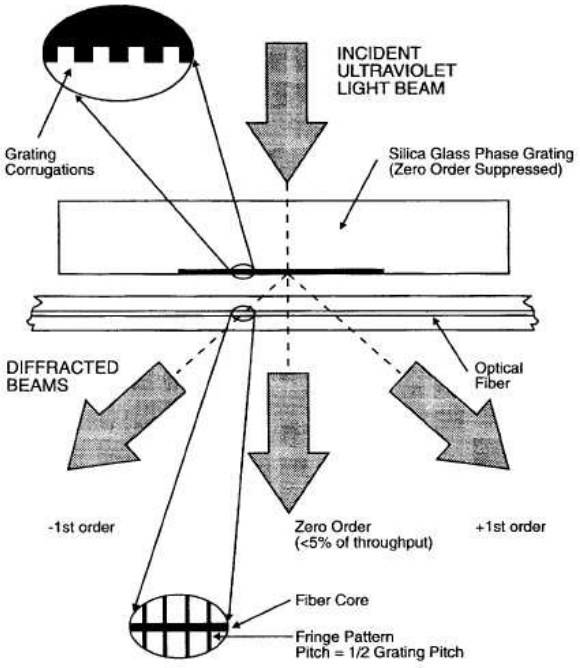

Figure 4.1. *Fiber Bragg grating fabrication apparatus based on a zero-order nulled diffraction phase mask[10].*

The fabrication techniques used in the beginning of the FBGs development(the internal writing and the holographic ones), have been today widely

replaced by the phase mask technique. A phase mask is substantially a flat slab of silica glass with a diffraction grating structure etched on one of its surfaces. It is usually designed so that a normally incident beam of ultraviolet light will be diffracted solely in the ± 1 orders in equal parts. The two ± 1 diffracted orders will interfere in a region close to the mask, giving rise to a periodic pattern. This pattern permits to write a grating structure in a fiber placed at the proper distance, as it is depicted in Figure 4.1.

The typical spectral response of a FBG with uniform index modulation exhibits secondary maxima on both sides of the main reflection peak. To prevent this often-undesired characteristic, it is possible to give a bell-like functional shape to the index modulation, performing what is referred to as apodization.

Using the phase mask technique it is also possible to produce chirped (variable grating period) or aperiodic gratings.

For an exhaustive treatment of the subject the reader is suggested to see [11].

4.2 Theory overview

Many works have been dedicated to the theoretical description of fiber Bragg gratings [12]. The most commonly used mathematical model is the coupled mode theory. It regards the grating as a weak perturbation on the fiber that couples power between forward and backward moving modes. Moreover, the difference of index of refraction between the core and the cladding of the fiber is assumed to be very small (weak guiding, or scalar wave approximation), so that both the electric and the magnetic field amplitudes can be considered perpendicular to the direction of propagation, satisfying the planar wave equation. This model provides two first-order differential equation (the coupled mode equations), which have to be satisfied together with two appropriate boundary conditions. In case of uniform or weak gratings there exists a closed-form solution of the problem.
To compute the reflection and transmission spectra of nonuniform gratings a number of other methods can be used. In the transfer matrix method, which is usually preferred, the FBG is approximated as a collection of a sufficient number N of sections, each of constant period and modulation. The fields at the two ends of a section can be related through a matrix. The overall spectra are then simply obtained through the overall transfer matrix, which is the product of the single transfer matrixes.

4.3 Applications

Fiber Bragg gratings have already a big number of important applications and their potential is still being tested in many fields.

The simplest application is the use of a FBG as a narrow-band mirror

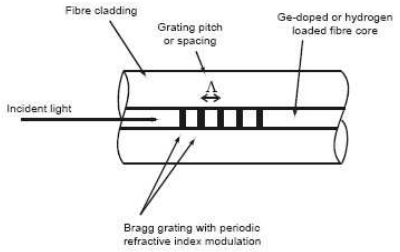

(a) Schematic drawing of a FBG.

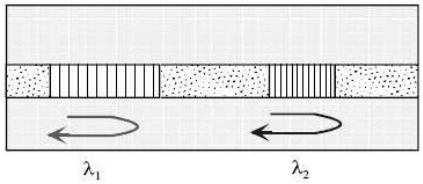

(b) FBGs as narrow-band mirrors.

Figure 4.2

which reflects the light in a desired wavelength interval. Writing more gratings in the same fiber, it is possible to increase and manipulate the reflected spectrum.

In the telecommunications field, FBGs provide a good solution to compensate for chromatic dispersion, which is the consequence of the different velocities of the various spectral components of a pulse that travels in an optical fiber. This is achieved with a chirped grating, i.e. a grating whose period changes along the axis of the fiber.

Very interesting and promising is the use of FBGs for sensing applications. The principle is that a change in strain, temperature or pressure will change in a predictable way the grating pitch Λ and the refractive index n of the fiber, shifting the peak of the reflected light (Bragg wavelength). FBG sensors can provide excellent performance, in terms of accuracy, sensitivity and immunity to electromagnetic and radio-frequency interference, being at the same time compact and potentially low cost. Strain and temperature sensors based on FBGs are already commercially available, while other sensors based on similar principles (accelerometers, magnetic sensors...)are currently being studied.

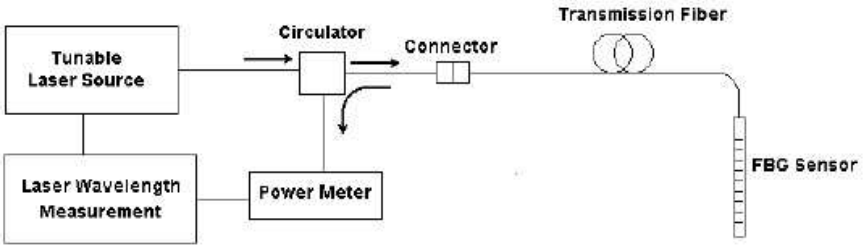

Figure 4.3. *Scheme of a FBG-based sensor.*

In the present work the principle behind a FBG sensor is used in a different way. The Bragg wavelength dependence on the temperature or strain is exploited to tune the diode laser, i.e. the FBG provides the frequency-tunable feedback to the diode laser. The most significant work on such a system so far is [13].

4.4 Tuning of FBGs

As was pointed out in the previous paragraph, the Bragg wavelength of a FBG can be tuned over a certain range by different means. This allows the FBG to work as a sensor or, as in the present work, as the frequency-selective element in a ECDL configuration. The Bragg wavelength is related to the grating period Λ and the refracting index n according to:

$$\lambda_B = 2\Lambda n \tag{4.1}$$

A variation of λ_B can thus be generally expressed as:

$$\Delta\lambda_B = 2n\Delta\Lambda + 2\Lambda\Delta n = \lambda_B(\frac{\Delta\Lambda}{\Lambda} + \frac{\Delta n}{n}) \tag{4.2}$$

Applying strain to a FBG, either pulling or compressing it, the Bragg wavelength is shifted. This is due to both the variation of the grating pitch and the variation of the refracting index caused by the elasto-optical effect, and it happens according to:

$$\Delta\lambda_{BS} = \lambda_B(1 - \rho_a)\Delta\varepsilon \tag{4.3}$$

where ρ_a is the photo elastic coefficient of the fibre, given by:

$$\rho_a = \frac{n^2}{2}[\rho_{12} - \upsilon(\rho_{11} - \rho_{12})] \tag{4.4}$$

Here ρ_{11} and ρ_{12} are the components of the fiber elasto-optical tensor and υ is Poisson's ratio. Typical values for the sensitivity to an applied axial strain are 1 nm/millistrain at 1300 nm and 0.64 nm/millistrain at 820 nm.

The temperature sensitivity of a FBG is primarily due to the thermo-optic effect, and to a minor extent to thermal expansion. The variation of Bragg wavelength in this case is expressed as:

$$\Delta\lambda_{BT} = \lambda_B(\xi + \alpha_F)\Delta T \tag{4.5}$$

where α_F is the thermal expansion coefficient and ξ the thermo-optic coefficient.

FBGs also exhibit a small sensitivity to pressure fields and low-frequency acoustic signals, which is rather difficult to exploit.

5 Tunable diode lasers

5.1 Diode lasers

Nowadays, the diode laser is becoming an indispensable device. Not only it is used in several consumer applications, such as compact disc players, laser printers and optical memories, but it is often a cheap and reliable alternative to more complex and expensive laser systems in laboratory work. The great value of diode lasers is in their compactness, reliability, ease of operation and low prize.

5.1.1 Fundamentals

Today the most popular diode laser architecture is the double heterostructure one, where the active medium is sandwiched between two cladding layers with slightly higher energy bandgap. Lasing is achieved by applying a forward bias current, which inject electrons and holes into the active layer, where they remain confined because of the energy barrier between the active and cladding layers. Population inversion is thus achieved between the almost full conduction band and the nearly empty valence band, providing the gain mechanism which produces the lasing action via electron-hole recombination.

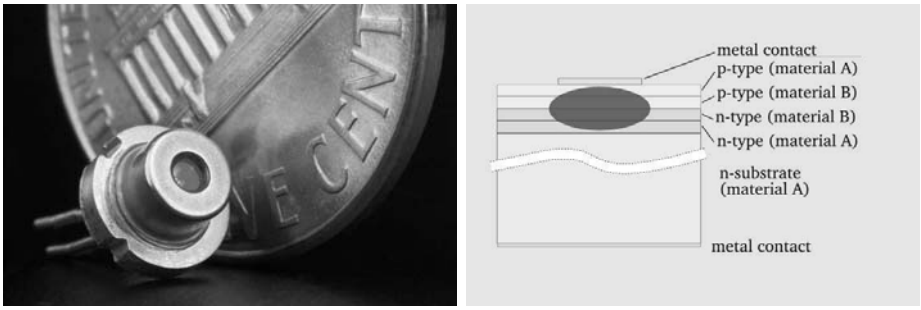

(a) *Picture of a typical diode laser[14].* ***(b)*** *Scheme of a double heterostructure diode laser[14].*

Figure 5.1

The crystal end facets form a Fabry-Perot resonator, which allows the existence of a finite number of longitudinal modes separated by:

$$\Delta\nu_{FSR} = \frac{c}{2nL} \tag{5.1}$$

, where c is the speed of light, n the refractive index of the semiconductor material and L the length of the cavity. As the gain spectrum linewidth is

much broader than the longitudinal mode separation(also called "free spectral range"), the diode laser can oscillate simultaneously in several different longitudinal modes. The lasing behavior, single mode or multimode, is strongly dependent on the fabrication technology.

Single transversal mode emission can be ensured by making the lateral dimensions of the active region small. This is usually achieved either by gain guiding or by index guiding.
In gain guided diode lasers the current flow is spatially confined, producing gain only in a narrow Gaussian-shaped stripe of the active layer, which acts like a waveguide for the light. In such structures the transverse mode confinement is not very effective and the width of the gain region results dependent on the current magnitude.
Index guided structures are generally more effective, as a true optical waveguide is built by fabricating stripes of material of lower refractive index adjacent to the gain region.

Many different diode laser architectures have been developed during the last decades. It is worth to mention the DFB (distributed feedback) diode laser, where a Bragg grating structure is fabricated alongside the active layer of the diode through a periodic perturbation of the refractive index and/or the gain of the laser medium itself, providing feedback only for a specific wavelength, while all other wavelengths suffer higher losses. If the grating structure is instead fabricated just outside the gain medium the device is referred to as a DBR (distributed Bragg reflector) diode laser. Another interesting architecture is the VCSEL (Vertical cavity surface emitting laser) one, where the optical cavity axis is along the direction of current flow, i.e. the length of the active region is the thickness of the active layer, which being very thin produces a high FSR. DFB and VCSEL diode laser are often chosen also for gas sensing applications [15].
However, it is not a purpose of this work to go in depth into the description of the various diode laser architectures, and the reader is referred to [16] for an exhaustive treatment of the subject.

5.1.2 Tunability and mode hopping

Typically, the laser wavelength can be tuned changing either the temperature or the injection current of the diode. The temperature dependence of the wavelength is a direct consequence of the shift of the optical gain curve and, usually to a minor extend, of the simultaneous variation of the optical path length (L x n) of the cavity with temperature. For instance, the QLD-760-10S diode from Qphotonics used in the present work showed a temperature dependence of about 0.07nm/°C. The laser can be tuned also varying the refractive index of the active region. This is achieved through ohmic heating of this region, simply changing the injection current. The current dependence of the QLD-760-10S diode was about 0.025nm/mA.

Unfortunately, the range over which it is possible to tune diode lasers is usually seriously reduced by discontinuous jumps in the emission wavelength. This phenomenon, known as mode hopping, is the result of competition between the longitudinal cavity modes that lie within the laser gain bandwidth. To tune the diode laser implies to vary the optical path length of the cavity and thus to shift the position of the modes. During the tuning process, one mode can thus happen to have more power than the original one and start suddenly to dominate, resulting in a discontinuous change in wavelength. As a further consequence, there appear intervals of wavelength that are not accessible. Sometimes this last problem can be solved or reduced using different combinations of temperature and injection current. Mode hopping drastically limits the performances of diode lasers as instruments for spectroscopic gas analysis, especially in the case of measurements at high pressures, when the effects of collisional line-broadening require a wider range of continuous tunability[17]. The wavelength vs. temperature plot for the QLD-760-10S diode in Figure 6.3 shows the typical behavior just described.

5.2 External cavity laser diodes

The development of external cavity configurations increased dramatically the potentials of diode lasers, making them an extremely attractive source of tunable light. The first reasonably simple ECDLs were developed in the early 1980s, thanks especially to the work of Littman, Liu and Metcalf. Today, ECDLs are an unreplaceable resource for spectroscopists and they are also being tested in many other industrial application, such as remote optical sensing.

5.2.1 Principles

In an ECDL, the optical feedback provided by an external frequency-selective element is coupled back into the diode cavity. This condition brings a number of important advantages. The diode can be forced to oscillate on a specific single mode (locking), reducing drastically the power distributed on the other modes. It can thus be tuned, varying the feedback frequency, over a wavelength range that is usually wider than that achievable by temperature and current tuning. Moreover, the emission linewidth of a locked diode is greatly reduced compared to the free-running case[18].
The two most common ECDL configurations are Littrow and Littman. It is convenient to give a brief description of them, before going more in depth into the behavior of a diode laser in an external cavity configuration.

5.2.2 Littrow configuration

In the Littrow configuration, whose scheme is shown in Figure 5.2, a reflective diffraction grating at its Littrow angle is aligned with the laser beam, so that

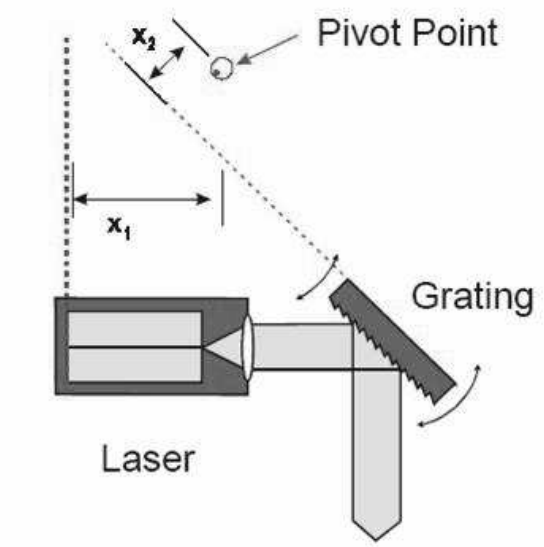

Figure 5.2. *Scheme of a system in Littrow configuration.*

the first diffracted order is reflected back into the diode. The output of this system is the zero order reflected beam. Tuning can thus be achieved by tilting slightly the grating , which implies to vary the wavelength of the feedback. This configuration is very simple and can offer a high output power. However, using a reflection grating, the angle of the output beam will change as the grating is tilted. This is usually referred to as a weak point of this configuration, but it can be overcome choosing an appropriate partly transmitting grating, so that the fixed zero-order transmitted beam becomes the system output. This has been done in the present work, as well as in some previous ones.

5.2.3 Littman configuration

The Littman configuration[19], shown in Figure 5.3, utilizes a grating tilted at grazing incidence. The first diffracted order is sent to a mirror, which reflects it back into the diode. The external cavity is thus formed between the diode rear facet and the mirror, whose angle can be varied to change the wavelength of the feedback and tune the diode. The zero reflected order, which is again the output of the system, remains unchanged as the mirror is tilted. However, the maximum power obtainable in the output is reduced by the fact that the beam is actually diffracted twice by the grating. This configuration can produce very high performances, but its design is rather complex and it requires a very fine mechanics.

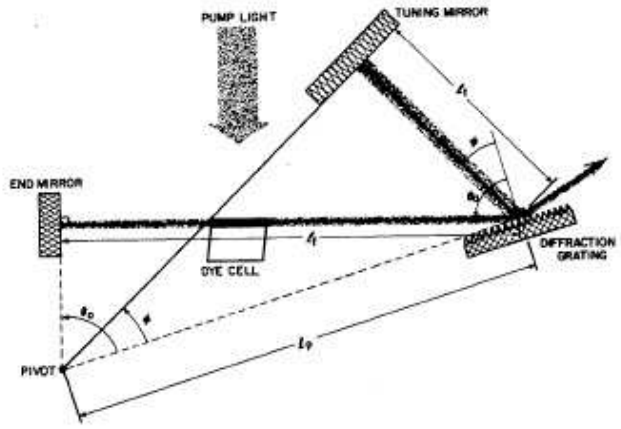

Figure 5.3. *Scheme of a system in Littman configuration, taken from the original paper in which it was proposed[19].*

5.2.4 Mode structure and continuous tuning

Schematically, an ECDL consists in two coupled Fabry-Perot cavities. The internal cavity, i.e the diode laser, is coupled to a usually much larger external cavity, which in the simple Littrow configuration is comprehended between the diode front facet and the diffraction grating.

The spectral structure of the composite cavity is rather complex, and it is strongly dependent on the residual reflectivity of the diode front facet and on the feedback strength. The front facet residual reflectivity is a key parameter. For an uncoated GaAlAs diode laser it is about 30%, but it can be reduced down to values as low as 10^{-5} with high quality anti-reflection(AR) coatings. The feedback strength depends obviously on the grating efficiency, whose different aspects have been treated in Chapter 3.

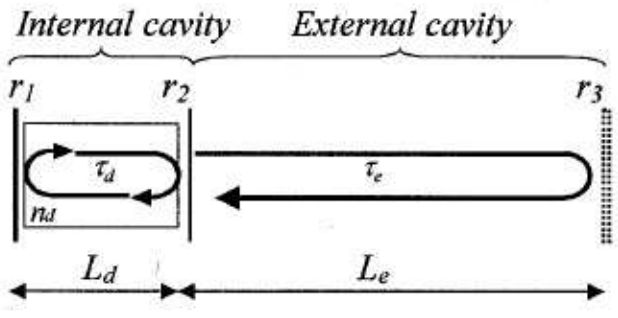

Figure 5.4. *Coupled-cavity model[20].*

In the ideal case, the diode should work just as a gain medium, i.e. the FP modes of the semiconductor crystal should be decoupled from the laser oscillator cavity. This would be possible only with an ideal AR coating with zero residual reflectivity.

In all practical situations, the spectral structure of the system will still include the modes of the internal cavity. However, around each mode there will be a "band" of very closely spaced modes, which are due to the external cavity. The lower the front facet residual reflectivity, the larger the width of these "bands". An increase of the feedback will also produce a similar effect. To get a quantitative feeling, it is worth to remember that the typical FSR of a diode laser (Equation (5.1)) is around 100GHz, while the FSR of a 15cm external cavity ($n \simeq 1$ in air) is just 1GHz.

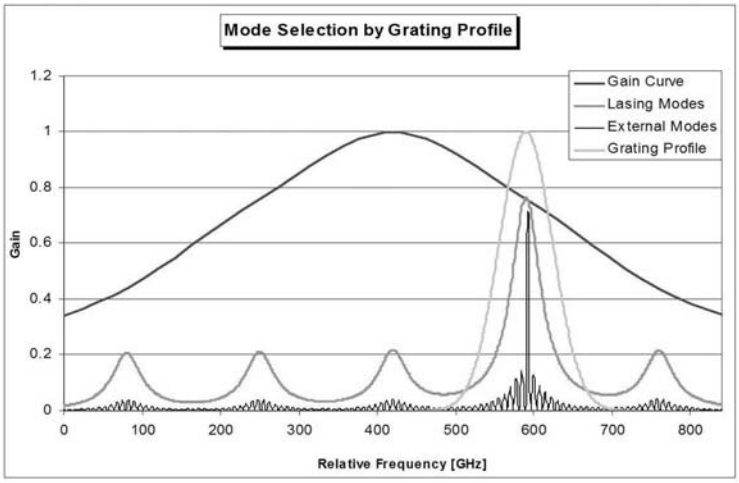

Figure 5.5. *Schematic representation of the spectral structure of the composite cavity.*

The grating, inducing a redistribution of the gain over the spectral structure, acts as a sort of mode selector. Typically, the dispersion FWHM of the grating is smaller than the FSR of the diode, but quite bigger than the FSR of the external cavity. A single external mode can thus not be precisely selected, i.e. it is not an easy task to control which external cavity mode gets a dominant dispersive feedback. In some papers (e.g. [20]) it is stated that the external cavity mode that will lase is the one with the minimum threshold gain. However, this assertion has been refuted in other works, which proved that the lasing external cavity mode will be the one closest to the frequency of the solitary laser, i.e. the laser without feedback. For a complete treatment of these aspects see [21].

According to what it has been written so far, it seems that a continuous

tuning of the system is not achievable. As a matter of fact, solely rotating the grating one can obtain, in the best case, a tuning that occurs in form of jumps between the closely spaced external cavity modes. For many applications this is not good enough and a continuous tuning is required.

Continuous tuning is actually achievable by varying the external cavity length in the appropriate proportion while the system is being tuned. In fact, changing the external cavity length makes the comb of the external cavity modes shift continuously away from its starting position. If the grating angle is thus scanned with the right synchronism, the dispersive feedback curve moves together with the external modes and one obtains a continuous tuning[22]. In both Littrow and Littman systems this is implemented by choosing a proper pivot point, around which the grating or the tuning mirror is tilted (Figures 5.2 and 5.3). This require a very fine mechanics and the maximum continuous tuning range achievable is of the order of a few tens of GHz [23]. However, improvements can be obtained with a simultaneous electronic control of the diode laser current [24].

6 Experiments

In all the experiments, the aluminum mount of the diode laser is thermally controlled through a Peltier element and an AD-590 sensor. These two elements are connected to a temperature controller (ILX Lightwave LDT-5910B), which allows to vary the temperature with a resolution of 0.1°C. The driver of the diode laser is a LDC2000 of ThorLabs, used in constant current operational mode. The spectral measurements have been carried out with a Hewlett Packard 86140A optical spectrum analyzer(OSA), whose maximum resolution is 0.06nm. A single lens with f=2mm was mounted on a translational stage and used to collimate the output beam.

6.1 Diode laser characterization

Three diode lasers model QLD-760-10S from QPhotonics have been used in the present work. The characteristics of the three samples are slightly different from each other, lying generally inside the tolerance intervals found in the manufacturer's data sheet (Figure 6.1). All the measurements reported in this paragraph have been carried out with the same diode.

Optical and Electrical Parameters (T = 25 °C)

Parameter		Symbol	Min	Typical	Max	Unit
Optical output power		P_{opt}		10	12	mW
Peak wavelength		λ	757	760	763	
Emitting area		WxH		3x1.5		µm x µm
Threshold current		I_{th}		55	60	mA
Operating current		I_f		80	100	mA
Forward voltage		U_f		2.4		V
Beam divergence	perpendicular	$^{\perp}\theta$	25	30	35	deg
	parallel	$^{\prime}\theta$	8	10	12	deg
Off Axis Angle		$\Delta\alpha\| \times \Delta\alpha\perp$			≤±3	deg
Positional accuracy		$\Delta X, \Delta Y, \Delta Z$			±100	µm
Spectral width (FWHM)		$\Delta\lambda$		1	1.5	nm
Mode structure			Single Transverse Mode			
Slope efficiency		dP_o/dI_{op}		0.7		mW/mA
Monitor current		I_m	0.15		4.0	mA

Figure 6.1. *Datasheet for QLD-760-10S diodes from QPhotonics.*

6.1.1 Power

The QLD-760-10S diode laser provides a maximum output power of about 10mW. For increasing temperatures, the threshold current increases and the emitted light power decreases, as it is shown in Figure 6.2. This behavior is a consequence of the increasing of scattering mechanisms with temperature. The device has not to be cooled down too much, in order to avoid condensation that might negatively affect its operation.

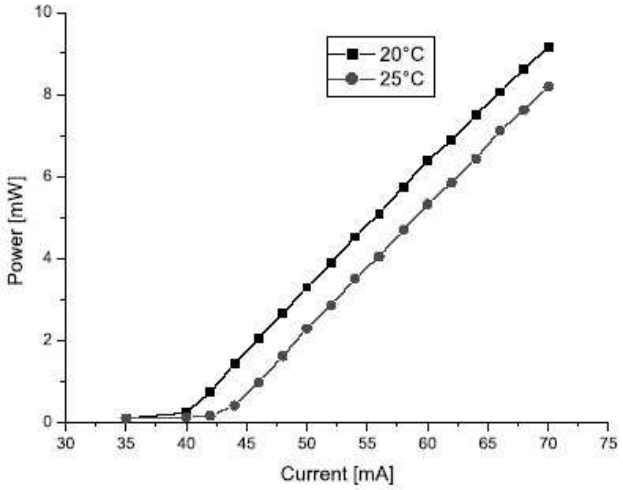

Figure 6.2. *Output power vs injection current curve at two different temperatures.*

6.1.2 Wavelength and tunability

The wavelength vs. temperature curve, shown in Figure 6.3, clearly illustrates the phenomenon of mode hopping. Tuning occurs in a rather discontinuous fashion, creating unreachable intervals of wavelength. The free spectral range of the diode, i.e. the spacing between the internal cavity modes, is:

$$\Delta\nu_{FSR} = \frac{c}{2nL} = 89.3\text{GHz}$$

6.1.3 Linewidth

The resolution of the optical spectrum analyzer ($\simeq 0.06$nm) limits the ability to determine the linewidth of the free-running diode. To get a better resolution, measurements have been carried out by means of a scanning Fabry-Perot interferometer(FPI).

First, it was checked that the diode was working in stable single mode operation. An optical insulator was collocated before the FPI, to avoid undesired feedback to the diode. The FPI was then aligned, sending the output to a fast photodiode. The aligning procedure of this instrument is a little tricky and it might take some time. A mirror spacing of $d = 32$mm was used for this measurement. The peak voltage of the ramp generator and the time scale of the oscilloscope were adjusted to obtain two output peaks in one single scan period, as it is shown in Figure 6.5. Since the free spectral

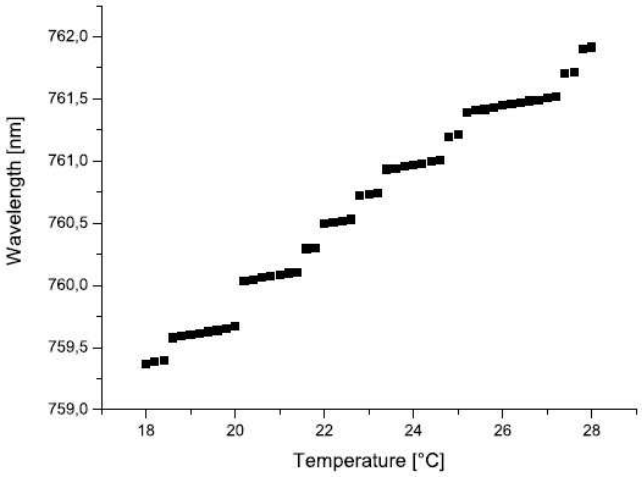

Figure 6.3. *Wavelength vs temperature plot.*

range(FSR) of the FPI is simply:

$$\Delta\nu_{FSR} = \frac{c}{2d} = 4.68\text{GHz}$$

we can calibrate the distance in time scale between the two peaks in the oscilloscope and thus obtain the linewidth.
The linewidth of the free running diode at 55mA and 20°C was measured to be:

$$\Delta\nu_{FWHM} = 450\text{MHz}$$

or, equivalently:

$$\Delta\lambda_{FWHM} = 0.86\text{pm}$$

6.2 Littrow-like configuration

A special mount was built to hold the silicone grating (Figure 6.4). The grating is clamped between two pairs of small metallic plates, and stretching is achieved either coarsely, by means of a micrometric screw, or finely, through a piezoelectric element. The mount allows also to rotate the grating around the two axes perpendicular to the beam direction. The transmitted beam, i.e. the output of the system, is sent directly to the spectrum analyzer. When working at currents close to threshold, which can be convenient as the diode laser is more sensitive to feedback in that region, it can be necessary to use a lens before the sensor, to increase the power coupled into it. The alignment of the system is first done manually, simply fixing the mount so that the first diffracted order goes approximately back into the diode. Then,

good alignment is achieved by finely controlling the grating angles through the apposite mount screws, while constantly checking the laser spectrum. The confirmation of a good alignment comes from an increase in the output power and an improved suppression of the side modes, together with a change in the lasing wavelength (unless accidentally the diode gets locked at the same wavelength it was emitting before).

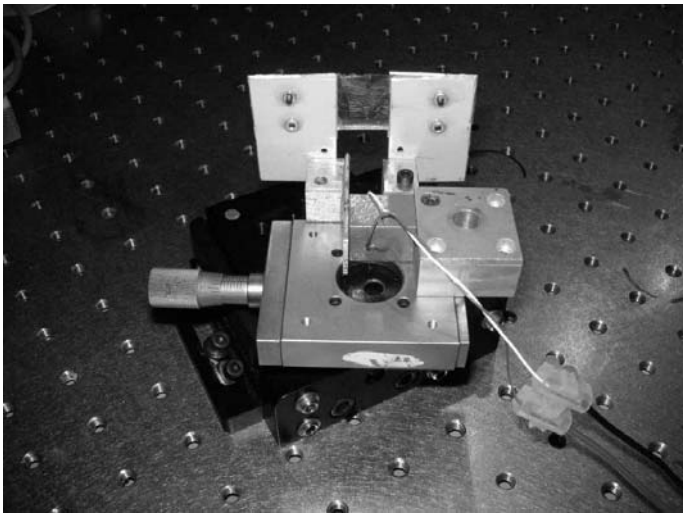

Figure 6.4. *The holder built for the silicone gratings.*

6.2.1 Locking

Thanks to the high efficiency of the grating, the locking of the diode is rather easily achieved. Given the 15% transmission of the grating, the laser gives enough output power to be easily detected and used. The grating used in these experiments was sample number 5, whose optical properties are reported in Figure 3.6.

The linewidth of the locked diode is expected to be considerably reduced compared to the free-running case. Measurements with the Fabry-Perot interferometer were thus carried out, in the same way described in Paragraph 6.1.3, with the diode locked at 758.327nm. Using a mirror separation of 37mm, it resulted:

$$\Delta\nu_{FWHM} = 310\text{MHz}$$

or, equivalently:

$$\Delta\lambda_{FWHM} = 0.60\text{pm}$$

In Figure 6.5b is reported the oscilloscope output. However, this result is limited by the resolution of the FPI, and can thus be considered just as an

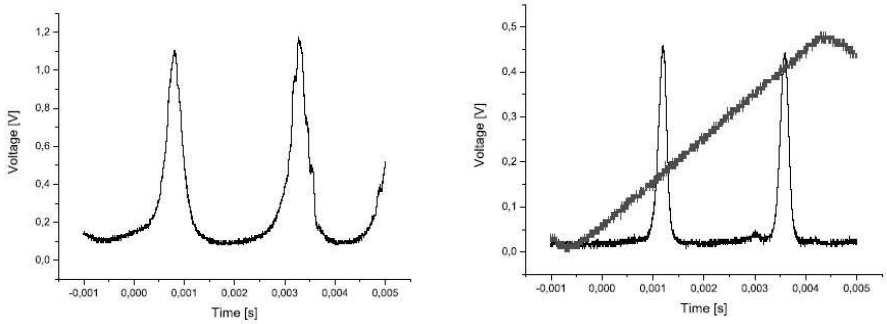

(a) Measurement of linewidth for the free-running diode.

(b) Measurement of linewidth for the locked diode.

Figure 6.5

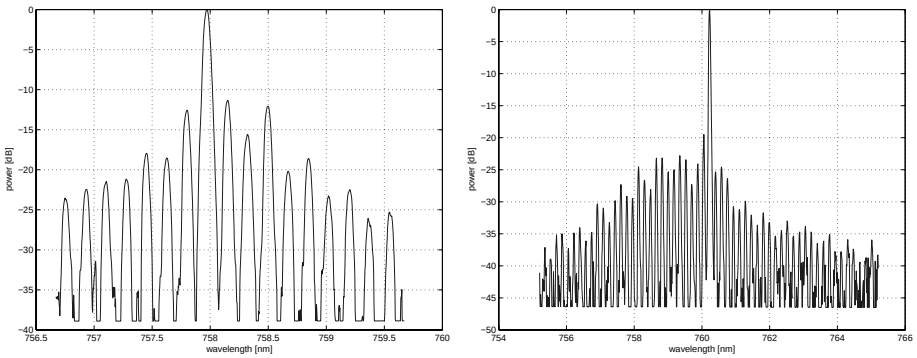

(a) Output spectrum of the free-running diode.

(b) Output spectrum of the locked diode.

Figure 6.6

upper boundary on the linewidth of the locked diode. In other words, the measured linewidth is the one of the Fabry-Perot cavity of the interferometer.
This fact can be proved in a simple way. Tilting slightly the FP interferometer, one causes a decrease in the mirror reflectivity, which results in a lower finesse F. Recalling that $\Delta\nu = \nu_{FSR}/F$, a decrease if the finesse will thus correspond to a larger FP linewidth. If the FP linewidth were much narrower than the linewidth of the laser, a small increase of the former one should not affect significantly the measurement. As this is not true for the present system, one can infer that the FP linewidth must be larger than that of the laser.

The oxygen measurements carried out subsequently , reported in Paragraph 6.2.3, gave a further confirmation of what just affirmed. It was possible

to detect two oxygen A-band absorption lines, which have a linewidth of approximately 3.5 GHz at ambient pressure. As a rule of thumb, the laser linewidth has to be at least about ten times narrower than the absorption line in order to get a reasonable measurement. The good quality of the results obtained thus confirms the previous estimate on the linewidth of the locked diode, i.e. $\Delta\nu_{FWHM} < 310$MHz.

As one can see in Figure 6.6, the side modes suppression is about 20dB, which means an order of magnitude higher than the free-running case.

6.2.2 Stretch tuning

In a classical Littrow configuration, the system is tuned by tilting the grating. However, as it appears from Equation (3.3), it is possible to achieve the same result by changing the grooves spacing d instead, i.e. stretching or compressing the grating. This is the basic idea behind this setup and it is made possible by the characteristics of the silicone gratings described in Chapter 3.

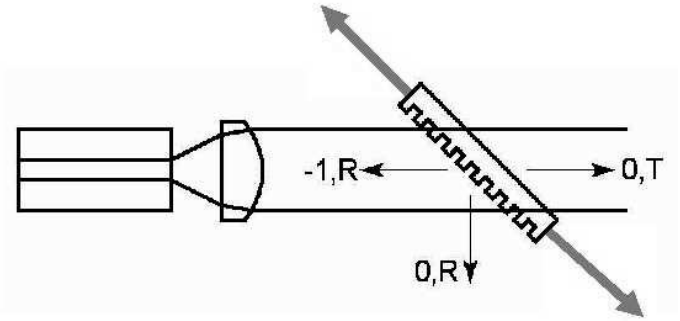

Figure 6.7. *Scheme of the Littrow-like system tuned by stretching of the grating*

The diode was locked at the wavelength for which the side modes suppression was highest. In order to be able to increase and decrease the groove spacing, the grating has to be slightly under stretch from the beginning. Stretch tuning is then achieved by finely controlling the piezoelectric element.

The results give a clear demonstration of the validity of this technique. The grating used had a groove frequency of 1800 lines/mm and the length of the external cavity was set to 25cm. The diode could be tuned over a 1.05nm range (Figure 6.8), with a grating strain of about 0.15%.

Unfortunately, the anti-reflection coating of the diode laser turned out to be insufficient, seriously limiting the performances of the system. The residual reflectivity of the front facet of the diode, declared to be about 2% by the manufacturer, makes the internal cavity mode structure dominant to

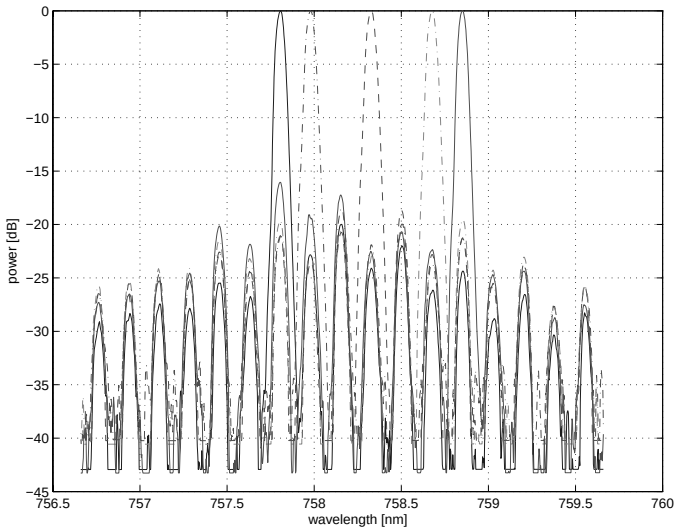

Figure 6.8. *Tuning achieved by stretching of the grating.*

the external one. As a result, tuning occurs substantially in form of regular jumps between the internal cavity modes.

As it is shown in Figure 6.9, the theoretical behavior, i.e. $\frac{\Delta\lambda}{\lambda} = \frac{\Delta d}{d}$ is closely followed. This means that the grating period varies very uniformly during the stretching process in the considered range. The grating can ac-

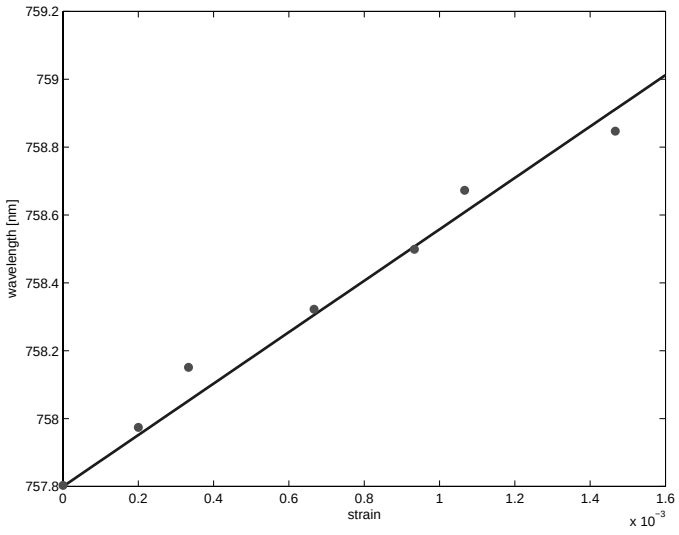

Figure 6.9. *Wavelength vs grating strain. Measured points plotted over theoretical curve*

tually be stretched much more than what it resulted useful to tune the diode. Stretching up to 10% of the initial length has been tried, with a good preservation of the quality of the reflected orders and a sensible progressive deterioration of the shape and power of the transmitted beam.

6.2.3 Oxygen measurements

The insufficient AR-coating of the diode made it impossible to perform oxygen measurements by means of the novel tuning technique described in the preceding paragraph.

Another approach was thus chosen. The grating angle is adjusted to lock the diode close to the desired absorption peak. Quasi-continuous tuning, i.e. tuning occurring in form of jumps between the very closely spaced external cavity modes, is then achieved by solely varying the injection current. This is sufficient to detect clearly the oxygen absorption peaks. It should be noticed, however, that in this system it is not possible to distinguish between a continuous and a quasi-continuous tuning behavior with the optical spectrum analyzer. The 25cm external cavity produces in fact a mode spacing of just 1.15pm(600MHz).

The major drawback of this method lies in the fact that the output power depends on the current. To overcome this problem a reference beam has to be extracted, and the absorption spectrum obtained from the ratio between the intensities of the signal and the reference beam.

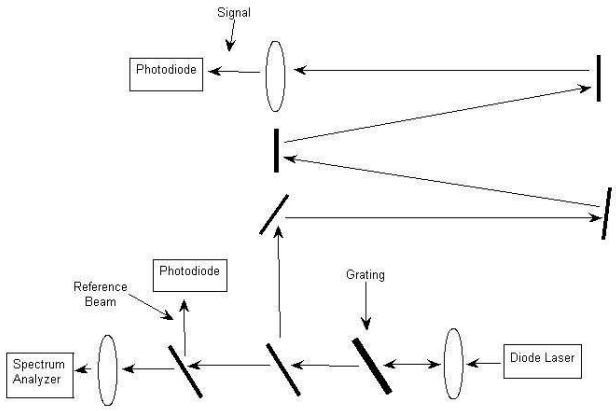

Figure 6.10. *Scheme of the setup used for the oxygen measurements.*

The setup used is depicted in Figure 6.10, where the optical path of the signal beam is about 10m. It was possible to scan over an interval of about 70pm, detecting two adjacent absorption peaks. In Figure 6.11 is reported

the measured spectrum, superimposed to the one obtained from HITRAN database. The agreement is very good, and the small wavelength shift could well be attributed to the calibration of the spectrum analyzer.

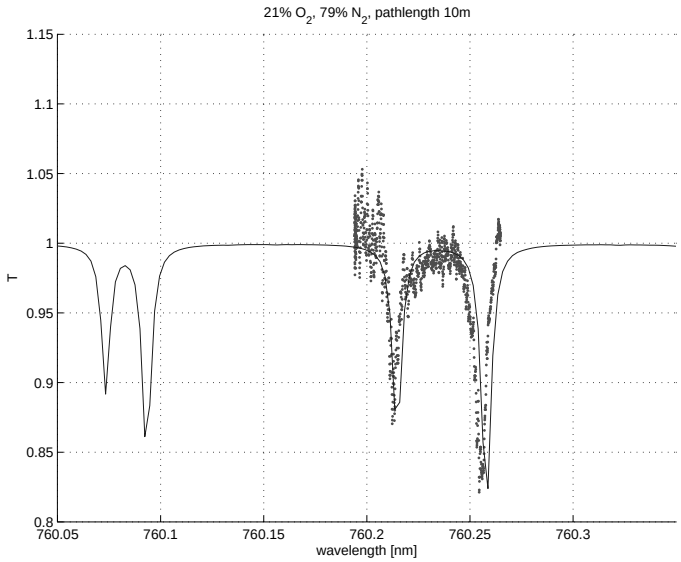

Figure 6.11. *Measured absorption spectrum plotted over the spectrum from HITRAN database.*

6.3 FBG configuration

Fiber Bragg gratings at 760nm are not standard devices and it has been extremely difficult to find a company capable of manufacturing them for a reasonable price. The devices were realized as a "best effort" and not all the required specifications have been exactly respected.

6.3.1 Coupling and locking

In this configuration the fiber is fixed to a X-Y-Z translational stage and the collimated beam is focused into the fiber core by means of a 10X microscope objective, which has a focal length of 16mm. Checking continuously the output power at the other end, the fiber is finely translated until the optimal position is reached. In this simple way it is possible to couple a little more than 50% of the light into the fiber, which is enough for this application.

The reflectivity spectrum of the FBG used in this system is shown in Figure 6.13. When the system was first conceived and designed, coupling losses were overestimated on purpose and a peak reflectivity of about 60% was requested, in order to guarantee sufficient feedback to the diode.

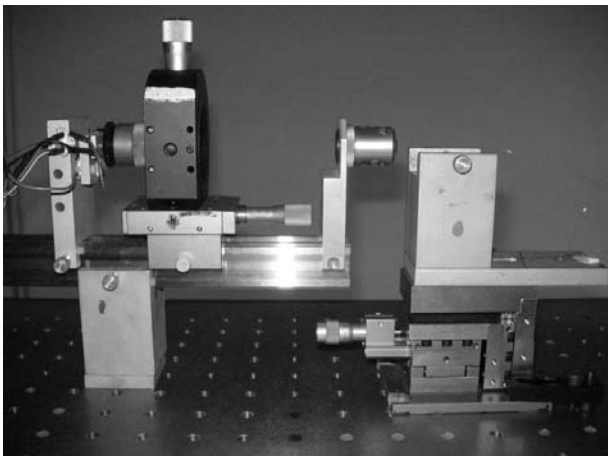

Figure 6.12. *Setup for coupling light into the fiber.*

A nice characteristic of this simple setup is that once the light is properly coupled into the fiber, the feedback produced by the FBG is automatically coupled back into the diode. The alignment of the second end of the fiber to the OSA sensor to monitor the output is extremely easy as well.

In Figure 6.14a is shown the output spectrum of the system when the gain curve of the diode does not overlap with the reflectivity curve of the FBG. In this case the output is very unstable, with several modes oscillating at the same time. This is due to the small secondary reflectivity peaks in the grating spectrum.

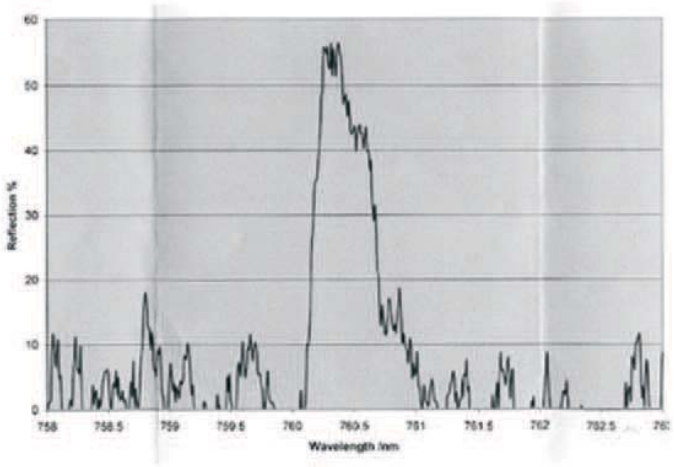

Figure 6.13. *Reflectivity spectra of the fiber Bragg grating.*

Locking is achieved when the principal reflectivity peak of the FBG lies in the gain region of the diode. A side modes suppression of about 20dB can be achieved. However, the behavior of the locked diode is not perfectly stable. The FWHM of the reflectivity curve of the grating is in fact about 0.6nm, much more than the FSR (0.17nm) of the internal cavity, whose modes structure is dominant as it has already been pointed out. Such a wide FWHM is more than double the value requested to the manufacturer in the FBG specifications and puts severe limits on the system tuning.

It has to be noticed that the feedback intensity achieved with this FBG is much more than the minimum needed to lock the diode. It could thus be possible to work with a FBG with much lower reflectivity (approximately up to 8 times lower), having most of the power available in the output.

6.3.2 Temperature tuning

For the fiber used the values for the thermal expansion coefficient and the thermo-optic coefficient are respectively:

$$\alpha_F = 0.55 \times 10^{-6}\ ^\circ\mathrm{C}^{-1}$$
$$\xi = 6.52 \times 10^{-6}\ ^\circ\mathrm{C}^{-1}$$

Remembering Equation (4.5), the shift in the Bragg wavelength is theoretically given by:

$$(\frac{\Delta\lambda_{BT}}{\lambda_B}) = (\xi + \alpha_F)\Delta T = 7.07 \times 10^{-6}\ \Delta T$$

To test the temperature tuning, the portion of the fiber with the grating was fixed in contact with a metal plate, which was thermally controlled by means of a Peltier element and an AD-590 sensor.

The insufficient AR-coating of the diode, which makes the internal mode structure dominant, and the large reflectivity bandwidth of the FBG complicated the tuning measurements. It was not possible to simply tune the grating by temperature, as then the output presented frequent and irregular jumps between modes.

The measurement was thus carried out in a different way. The FBG temperature was kept fixed and the gain curve of the diode was shifted continuously by temperature, sweeping over the grating reflectivity spectrum. A trace, obtained memorizing all the maximum values of the laser output during the sweep, was thus saved in the OSA. This same procedure was repeated for different temperatures of the FBG. In Figure 6.15 are shown three traces obtained respectively at 7°C, 27°C and 47°C. The distance between the rising fronts of the curves is measured to estimate the shift in the Bragg wavelength:

$$(\frac{\Delta\lambda_B}{\lambda_B})_{thermo} \simeq 6.6 \times 10^{-6}\ \Delta T$$

The agreement with the theory is good.

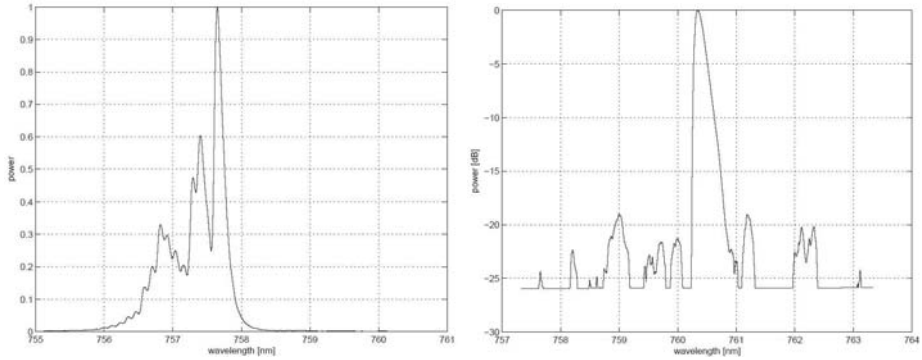

(a) *Output spectrum when the diode is not locked(linear scale).* **(b)** *Output spectrum of the locked diode(log scale).*

Figure 6.14

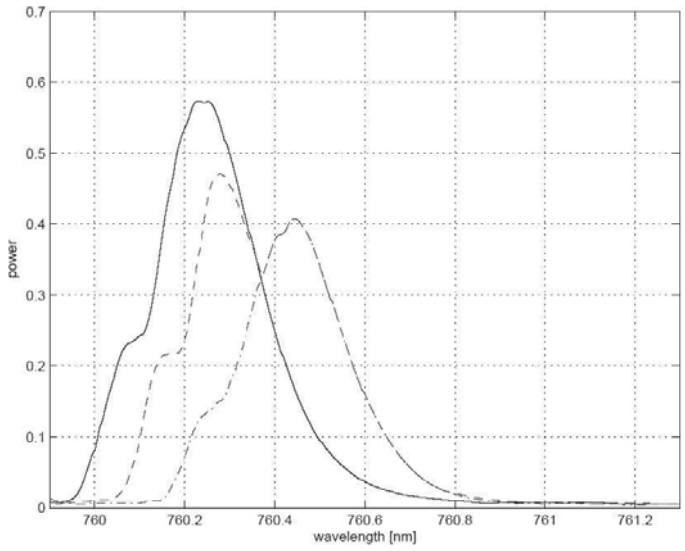

Figure 6.15. *Traces obtained memorizing the maximum spectral output while the diode gain curve is shifted, for three different temperatures of the FBG(respectively 7° C, 27° C and 47° C, from left to right).*

7 Conclusions and future perspectives

The obtained results undoubtedly encourage further research work.

The potentials of deformable optical components would deserve a particular attention. Molded silicone gratings made possible the realization of an innovative ECDL system, whose advantages and drawbacks should be better studied. Dynamic tuning of the system could also be tried, making the grating vibrate through, for example, a voice coil . The manufacturing technique of silicone gratings should be improved, and their possible use in other different applications should be explored. Moreover, other interesting optical elements could be fabricated with the same materials (deformable mirrors, lenses, etc..).

The FBG setup demonstrated the possibility to build a compact and simple oxygen sensor. However, FBGs at 760nm are not standard devices and at present day it is rather hard and expensive to get good quality samples.

The quality of the diode laser AR coating put serious limit to the quality of all the results, and it is thus the first aspect that should be improved in eventual future works.

References

[1] Gabriel Somesfalean. *Environmental monitoring using diode-laser-based spectroscopic techniques.* PhD thesis, Department of Physics, Lund Institute of Technology, SE-221 00 Lund, Sweden, 2004.

[2] William T. Silfvast. *Laser Fundamentals.* Cambridge University Press, New York, 2004.

[3] Anthony E. Siegman. *Lasers.* University Science Books, Sausalito,CA, 1986.

[4] H.D. Babcock and L. Herzberg. Fine structure of the red system of atmospheric oxygen bands. *Astrophysical Journal*, 108:167–190, 1948.

[5] D.Q. Wark and D.M. Mercer. Absorption in the atmosphere by the oxygen "a" band. *Applied Optics*, 4:839–844, 1965.

[6] G. Berden, R. Engeln, P. C. M. Christianen, J. C. Maan, and G. Meijer1. Cavity-ring-down spectroscopy on the oxygen a band in magnetic fields up to 20 t. *Physical Review A*, 58:3114–3123, 1998.

[7] http://cfa www.harvard.edu/HITRAN/. The hitran database.

[8] Christopher Palmer. *Diffraction grating handbook.* Erwin Loewen Editor, 2002.

[9] A.N. Simonov, O. Akhzar-Mehr, and G. Vdovin. Light scanner based on a viscoelastic stretchable grating. *Optics Letters*, 30:949–951, 2005.

[10] Kenneth O. Hill and Gerald Meltz. Fiber bragg grating technology fundamentals and overview. *Journal Of Lightwave Technology*, 15:1263–1276, 1997.

[11] Raman Kashyap. *Fiber Bragg Gratings.* Elsevier, 1999.

[12] Johannes Skaar. *Synthesis and characterization of fiber Bragg gratings.* PhD thesis, Norwegian University of Science and Technology, NO-7491 Trondheim, NORWAY., 2000.

[13] G. Karlsson, N. Myrèn, W. Margulis, S. Taccheo, and F. Laurell. Widely tunable fiber-coupled single-frequency er-yb:glass laser. *Applied Optics*, 42:4327–4330, 2003.

[14] http://en.wikipedia.org. Wikipedia, the free encyclopedia.

[15] V. Weldon, J.O'Gorman, J.J. Perez-Camacho, D. McDonald, J. Hegarty, J.C. Connolly, N.A. Morris, R.U. Martinelli, and J.H. Abeles. Laser diode based oxygen sensing: a comparison of vcsel and

dfb laser diodes emitting in the 762nm region. *Infrared Physics and Technology*, 38:325–329, 1997.

[16] P. Agrawal and N.K. Dutta. *Semiconductor lasers*. Van Nostrand Reinhold, New York, 1993.

[17] Jian Wang. New strategies of diode laser absorption sensors. Master's thesis, Stanford University, 2001.

[18] Govind P. Agrawal. Line narrowing in a single-mode injection laser due to external optical feedback. *IEEE Journal of Quantum Electronics*, 20:468–471, 1984.

[19] K.Liu and M.G. Littman. Novel geometry for single-mode scanning of tunable lasers. *Optics Letters*, 6:117–118, 1981.

[20] G. Genty, A. Grohn, H. Talvitie, M. Kaivola, and H. Ludvigsen. Analysis of the linewidth of a grating-feedback gaalas laser. *IEEE Journal of Quantum Electronics*, 36:1193–1198, 2000.

[21] B. Tromborg, J. Mork, and V. Velichansky. On mode coupling and low-frequency fluctuations in external-cavity laser diodes. *Quantum Semiclass. Opt.*, 9:831–851, 1997.

[22] S. Jin, Y. Li, and M. Xiao. Single-mode diode laser with a large frequency-scanning range based on weak grating feedback. *Appl. Opt.*, 35:1436–1441, 1996.

[23] T. Laurila, T. Joutsenoja, R. Hernberg, and M. Kuittinen. Tunable external-cavity diode laser at 650nm based on a transmission diffraction grating. *Applied Optics*, 41:5632–5637, 2002.

[24] C. Pedritis, I.D. Lindsay, D.J. Stothard, and M. Ebrahimzadeh. Mode-hop-free tuning over 80ghz of an extended cavity diode laser without antireflection coating. *Review of Scientific Instruments*, 72:3811–3815, 2001.